Isotropic-cholesteric phase transition of filamentous virus suspensions as a function of rod length and charge

Kirstin R. Purdy and Seth Fraden
Complex Fluids Group, Department of Physics, Brandeis University, Waltham, Massachusetts 02454, USA
(Received 9 June 2004; published 14 December 2004)

The viruses studied are genetically engineered, charged, semiflexible filamentous bacteriophages that are structurally identical to M13 virus, but differ either in contour length or surface charge. While varying contour length (L) we assume the persistence length (P) remains constant, and thus we alter the rod flexibility (L/P). Surface charge is altered both by changing solution *p*H and by comparing two viruses, *fd* and M13, which differ only by the substitution of one charged for one neutral amino acid per virus coat protein. We measure both the isotropic and cholesteric coexistence concentrations as well as the nematic order parameter after unwinding the cholesteric phase in a magnetic field as a function of rod surface charge, rod length, solution ionic strength, and solution *p*H. The isotropic-cholesteric transition experimental results agree semiquantitatively with theoretical predictions for semiflexible, charged rods at high ionic strength, but disagree at low ionic strength.

DOI: 10.1103/PhysRevE.70.061703 PACS number(s): 64.70.Md, 61.30.St

I. INTRODUCTION

For a suspension of rigid rodlike particles, Onsager determined that hard-core interactions alone are sufficient for inducing an entropy-driven phase transition from an isotropic phase, in which the particles are randomly oriented, to a nematic phase, in which the orientation of the particles is distributed about a preferred direction [1]. When the rodlike particles are semiflexible and/or charged, like many biopolymers such as DNA and F-actin, the properties of the phase transition can differ significantly from those predicted for hard, rigid rods. Small amounts of flexibility are predicted [2] and observed [3,4] to increase the stability of the isotropic phase and lead to a less ordered nematic phase. In this paper, we study the effects of flexibility on the isotropic-nematic (*I-N*) transition using suspensions of the rodlike charged, semiflexible M13 virus and M13 virus length-mutants. By varying the contour length (L) of our experimental charged rods while maintaining a constant persistence length (P), we change the rod flexibility (L/P). The persistence length is defined as the length over which tangent vectors along a polymer are correlated [5]. In our experiments, the flexibility of the rods remains within the semiflexible limit, where $P \sim L$. The effect of surface charge on the *I-N* transition of charged rods is also investigated. Surface charge is varied by modifying both the surface chemistry of the rods and the solution chemistry, by changing *p*H.

While Onsager developed the original theory for the isotropic-nematic transition of hard and charged rigid rodlike particles, Khokhlov and Semenov were responsible for incorporating flexibility into this theory [2]. They extended Onsager's theory to include systems of semiflexible rods with a large length (L) to diameter (D) aspect ratio (L/D) and arbitrary persistence length. They explicitly calculated the equilibrium properties of the *I-N* phase transition in the limit of very flexible $L/P \gg 1$ and very rigid $L/P \ll 1$ rods and interpolated between the two limits to find the properties of semiflexible rod phase behavior. Shortly afterwards, Chen numerically calculated the concentrations of the coexisting isotropic and nematic phases as well as the order parameter of the coexisting nematic phase for arbitrary flexibility using Khokhlov-Semenov theory [6]. For rigid rods, the limit of stability of the isotropic phase is predicted to be $c_i = 4/b$, where c_i is the number density and $b = \pi L^2 D/4$, the average excluded volume in the isotropic phase [7]. For flexible rods, Khokhlov-Semenov theory predicts that slight semiflexibility will increase the stability of the isotropic phase by increasing bc_i, and will narrow the *I-N* coexistence region. Flexibility is also predicted to significantly lower the nematic order parameter at coexistence. The nematic order parameter S is the second moment of the orientational distribution function of the rods, $f(\theta)$, or $S = 2\pi \int P_2[\cos(\theta)] f(\theta) d\theta$, where P_2 is the second Legendre polynomial. For a completely aligned nematic $S = 1$, whereas for an isotropic phase $S = 0$. For rigid rods the predicted nematic order parameter at coexistence is $S = 0.79$ [8]. The predictions from the Khokhlov-Semenov theory show quantitative agreement with the measured *I-N* transition for suspensions of charged semiflexible virus *fd*, charged polymer xanthan, and neutral polymer PBLG [3,4].

Electrostatic interactions are incorporated into the Onsager model by rescaling the bare rod diameter D to a larger effective diameter D_{eff} which depends on the ionic properties of the particle and the solution [1,9]. D_{eff} is calculated from the second virial coefficient of Onsager's free energy equation for charged rigid rods. In Fig. 1, we plot D_{eff} as described by Stroobants *et al.* [9] as functions of ionic strength and rod surface charge. The nonlinear Poisson-Boltzmann equation used in the Stroobants description of D_{eff} was solved numerically using the approximations developed by Philip and Wooding [10]. With increasing ionic strength, D_{eff} decreases approaching the bare rod diameter. Past experiments have shown that D_{eff} accurately describes the ionic strength dependence of the *I-N* transition of *fd* virus suspensions [3]. For highly charged rods, the effect of surface charge on D_{eff} is small as the nonlinear nature of the Poisson-Boltzmann equation leads to counterion condensation near

 ©2004 The American Physical Society

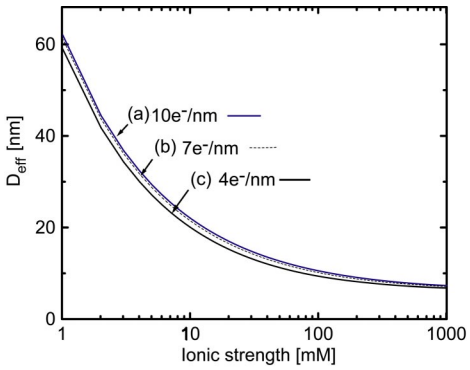

FIG. 1. (Color online) Effective diameter as a function of ionic strength and surface charge. With increasing ionic strength D_{eff} approaches the bare diameter of *fd* (M13) $D=6.6$ nm. The effective diameter is plotted for surface charges of 10 e^-/nm, 7 e^-/nm, and 4 e^-/nm. These surface charge densities are the same as those measured for (a) *fd* at *p*H 8.2, (b) M13 at *p*H 8.2 or *fd* at *p*H 5.2, and (c) M13 at *p*H 5.2. At these surface charge densities, D_{eff} is insensitive to variation in charge.

the colloid surface which renormalizes the bare surface charge to a lesser effective charge, which is nearly independent of the bare surface charge. In the nematic phase, the effective diameter increases due to an added effect called "twist," which is characterized by the parameter $h=\kappa^{-1}/D_{\mathrm{eff}}$, where κ^{-1} is the Debye screening length. The effect of twist on D_{eff}, however, is predicted to be small for *fd* [3], and we neglect it here. Studying the influence of ionic strength and surface charge on the *I-N* phase behavior tests if D_{eff} can be accurately used to map charged rod phase behavior to hard-rod theories.

Onsager's theory is based on an expansion of the free energy truncated at the second virial level, so that only two-particle interactions are considered. This assumption has been shown to be accurate in the limit of very long rods, where $L/D>100$ [11], or for very dilute suspensions. In our experimental system, however, decreasing the ionic strength rapidly decreases our effective aspect ratio to values far below the $L/D=100$ limit. In order to accurately predict the phase behavior of rods with an effectively small aspect ratio, the theoretical free energy needs to incorporate third and higher virial coefficients. Scaled particle theory (SPT), which incorporates all higher virial coefficients in an approximate way, is one theory which accomplishes this [12]. A scaled particle theory for hard rigid rods was originally developed by Cotter [12]. More recently, we have expanded this theory to include charge and semiflexibility [13,14]. In conjunction with the Khokhlov-Semenov second virial theory, we use this scaled particle theory to interpret our experimental results.

In this paper, we present experimental measurements of the isotropic-nematic phase transition of semiflexible charged colloidal rods as a function of rod length, surface composition, solution *p*H, and solution ionic strength. We measure both the coexistence concentrations and the nematic order parameter and compare our results to both Onsager's theory, by way of Chen's numerical calculation [6], and scaled particle theory. For our model rods, we use monodisperse suspensions of charged semiflexible rodlike *fd* virus, wild type M13 virus, and mutants of M13 virus which differ from the wild type only by their contour length. In solution, these particles exhibit isotropic, cholesteric (or chiral nematic), and smectic phases [3,15–17]. Suspensions of *fd* have been previously shown to exhibit an *I-N* transition which agrees with theoretical predictions for semiflexible rods with an effective diameter D_{eff} [3]. M13 virus is structurally identical to *fd* virus, differing only in surface charge, making these two particles an ideal system for studying the influence of bare surface charge on the isotropic-nematic transition. Additionally, by comparing the *I-N* phase behavior of each of the M13 mutants, which except for length are structurally identical, and therefore by assumption have the same persistence length, we measure the influence of flexibility, defined as the ratio L/P on this transition. Though *fd* and M13 exhibit a cholesteric phase, the free energy difference between the cholesteric and the nematic phase is much smaller than the difference between the isotropic and nematic phases [18]. This allows us to compare our results to theoretical predictions for the *I-N* transition. We refer to the cholesteric phase as the nematic phase henceforth.

Motivation for these length and surface charge dependent measurements of the *I-N* transition arose because new measurements of the nematic-smectic (*N-S*) transition in this same system [19] exhibit measurable surface charge dependence and ionic strength dependence which cannot be accounted for by treating the virus as a hard rod with a diameter D_{eff}, in contrast to our previous measurements, which were limited in range of ionic strength [16]. The new *N-S* measurements inspired a closer look at the ability of D_{eff} to describe the effects of surface charge on the *I-N* transition. New measurements of the *N-S* transition as a function of length also indicate that semiflexibility has no measurable effect on the *N-S* transition for the limited range studied, which is as predicted, but which is in sharp contrast to the large predicted effect of flexibility on the *I-N* transition for the same range. The measurements presented here of the *I-N* transition as a function of charge and flexibility will contribute to the understanding of the relative importance of these variables in the evolution of the liquid crystalline ordering of charged semiflexible rodlike particles with concentration.

II. MATERIALS AND METHODS

Properties of *fd* and wild type M13 include length $L=0.88$ μm, diameter $D=6.6$ nm, persistence length $P=2.2$ μm, and molecular weight $M=1.64\times10^7$ g/mol [20]. Each virus consists of approximately 2700 coat proteins helicoidally wrapped around single stranded DNA. The two viruses differ only by one amino acid per coat protein. In *fd* this amino acid is the negatively charged aspartate (asp_{12}), and in M13 it is the neutral asparagine (asn_{12}) [21]. Thus at near neutral *p*H, *fd* has one more negative charge per coat protein (3.4 ± 0.1 e^-/protein) than M13 (2.3 ± 0.1 e^-/protein), which results in a net charge difference of approximately 30% [22]. X-ray diffraction studies are unable to clearly discern any structural differences be-

TABLE I. Surface charge of *fd* and M13 at *p*H 8.2 and 5.2. (A) The charge of *fd* obtained by titration experiments [22]. (B) M13 has one less negative amino acid per coat protein than *fd*, thus the surface charge of M13 can be approximated by subtracting one charge per protein subunit from the *fd* surface charge values. (C) Ratio of electrophoretic mobility (m), determined from Fig. 2, of M13 to *fd*. (D) By multiplying the known *fd* charge by m, the linear surface charge density of M13 can be calculated. (E),(F) *fd* and M13 surface charge per unit length, respectively.

	A	B	C	D	E	F
*p*H	*fd* $e-$/subunit	M13 e^-/subunit (charge of *fd* minus 1)	mobility ratio mM13/mfd	M13 e^-/subunit (electrophoresis)	*fd* e^-/nm	M13 e^-/nm
8.2	3.4±0.1	2.4±0.1	0.67	2.3±0.05	10	7
5.2	2.3±0.1	1.3±0.1	0.5	1.2±0.05	7	3.6

tween M13 and *fd* [23]. The M13 length-mutants share the same properties as wild type M13, varying only in length and molecular weight, which scales linearly with length. The M13 mutant have lengths of 1.2 μm, 0.64 μm, and 0.39 μm. Wild type M13, *fd*, and M13K07 (the 1.2 μm mutant phage) were grown using standard techniques [24]. The other two mutant phages were grown using the phagemid method, which produces bidisperse solutions of the phagemid and the M13K07 helper phage [24]. We chose two plasmid DNA sequences, PGTN28 (4665bp) and LITMUS38 (2820bp) (New England Biolabs, Cambridge, MA) to form our phagemids of length 0.64 μm and 0.39 μm, respectively. Sample polydispersity was checked using gel electrophoresis on the intact virus and on the viral DNA. Except for the phagemid solutions, which contained approximately 20% by mass helper phage M13K07, the virus solutions were highly monodisperse as indicated by sharp electrophoresis bands.

In a bidisperse system of long and short rods, it is predicted that when isotropic and nematic phases are in coexistence, the longer rods will strongly partition into the nematic phase [25,26]. Using this fractionation effect, we attempted to purify the bidisperse suspensions of the phagemid and M13K07 helper phage. We observed partitioning of the long rods into the nematic phase by DNA agarose gel electrophoresis (two to three times more long rods in the cholesteric phase than in the isotropic phase, in qualitative agreement with Lekkerkerker *et al.* [25]), but were unable to successfully measure a difference in long rod concentrations in the isotropic phase after successive iterations of fractionation. The effect of fractionation on the coexistence concentrations was assayed by comparing the isotropic and nematic concentrations of coexisting samples (about 50% of each phase in one sample) with the highest concentrations for which the samples remained completely isotropic and the lowest concentrations for which the samples remained completely nematic, respectively. The only difference we observed was that the nematic concentration measured in coexistence with the isotropic phase was consistently about 5–10 % lower than the nematic concentration measured when the sample was 100% nematic. The lower concentrations in the coexisting nematic phases are due to the partitioned long rods undergoing the *I-N* phase transition at lower mass concentrations. Because the effect of bidispersity is small, we report the phase behavior for the 0.39 μm and 0.64 μm rods at the limits of the coexistence region with the understanding that the samples contain about ~20% (by mass) 1.2 μm rods.

All samples were dialyzed against a 20 mM Tris-HCl buffer at *p*H 8.2 or a 20 mM sodium acetate buffer adjusted with acetic acid to *p*H 5.2. To vary ionic strength, NaCl was added to the buffering solution. The values for surface charge of *fd* and M13 at *p*H 8.2 and *p*H 5.2 are presented in Table I. The surface charge of *fd* was determined by titration experiments [22], and the surface charge of M13 was calculated in two ways, both starting from the known *fd* surface charge. One way is to compare the molecular composition of *fd* and M13, and the second is to use the fact that because M13 and *fd* are identical except for their surface charge, their electrophoretic mobilities are proportional to the net surface charge [27]. In Fig. 2, we show using agarose gel electrophoresis of intact virus that *fd* migrates 200% faster than M13 at *p*H 5.2 and 150% faster at *p*H 8.2. Note in Table I we show that the surface charge of M13 at *p*H 8.2 is the same as the surface charge of *fd* at *p*H 5.2.

All measurements were done at room temperature. The virus concentrations were measured by absorption spectro-

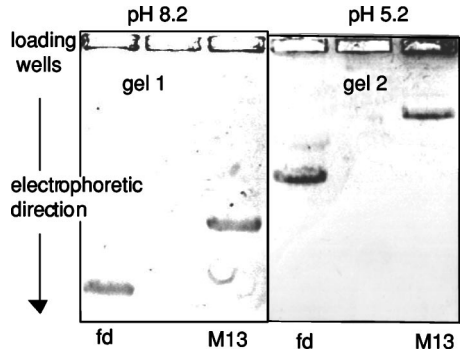

FIG. 2. Agarose gel electrophoresis of *fd* and M13 virus at *p*H 8.2 (gel 1) and *p*H 5.2 (gel 2). At *p*H 5.2 the buffer was 40 mM sodium acetate, and at *p*H 8.2 the buffer was 40 mM tris-acetate-EDTA (TAE). Gels were run at ~1.0% agarose concentration and ~3.5 V/cm for 4 h. Samples were placed in loading wells at a concentration of approximately 0.3 mg/mL. M13 and *fd* have the same length (L=0.88 μm) and diameter (D=6.6 nm), and differ only in surface charge. The ratio of electrophoretic migration distances between M13 and *fd* within each gel is therefore equal to the ratio of the surface charge. The electrophoresis bands for *fd* at *p*H 5.2 and M13 at *p*H 8.2 are not at the same migration distance, because the absolute migration distance is also a function of the buffer ions.

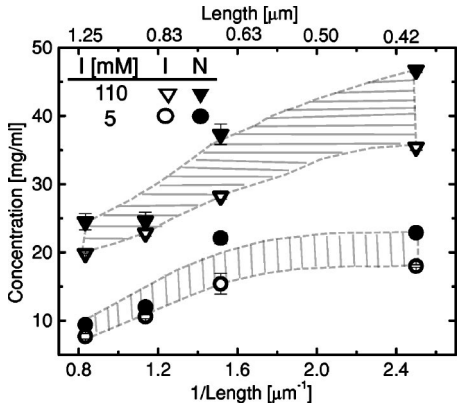

FIG. 3. Isotropic-nematic coexistence concentrations as a function of M13 mutant contour length at 5 mM and 110 mM ionic strengths at *p*H 8.2. Open symbols represent the coexisting isotropic phase and solid symbols the nematic phase. Shaded areas are a guide to the eye indicating the coexistence regions. For rigid rods, the coexistence concentrations $\rho_i \propto 1/L$ at a constant ionic strength (constant D_{eff}). Deviations from this relationship are most likely due to rod flexibility.

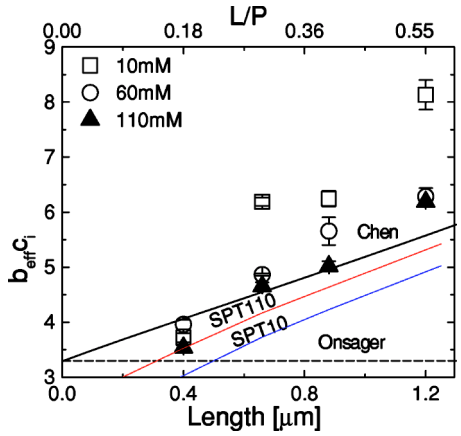

FIG. 4. Dimensionless concentration of the isotropic phase in coexistence with the nematic phase as a function of M13 mutant contour length for three ionic strengths at *p*H 8.2. The concentration is defined as $b_{\mathrm{eff}}c_i=(\pi/4)D_{\mathrm{eff}}L^2N_i/V=25.4\rho_i$ (mg/mL)L (μm)D_{eff} (μm). Scale on the top of the graph identifies the flexibility in terms of L/P with $P=2.2$ μm. If the rods are rigid, the phase behavior is predicted to be independent of length (Onsager) (dashed line). Semiflexible rods show increasing $b_{\mathrm{eff}}c_i$ with increasing flexibility as predicted by Khokhlov-Semenov theory calculated by Chen (solid line). Scaled particle theory at 100 mM ionic strength (SPT110) and at 10 mM ionic strength (SPT10) indicates that $b_{\mathrm{eff}}c_i$ depends on L/D_{eff}.

photometry with the optical density (A) of the virus being $A_{269\ \mathrm{nm}}^{1\ \mathrm{mg/mL}}=3.84$ for a path length of 1 cm. The nematic order parameter was obtained by unwinding and aligning the cholesteric phase in a 2T permanent magnet (SAM-2 Hummingbird Instruments, Arlington, MA 02474) [28] and measuring the sample birefringence. At 2T, the magnetic field has a negligible effect on nematic ordering [29,30]. The nematic order parameters were calculated from the optical birefringence measurements obtained with a Berek compensator using the equation $\Delta n_{\mathrm{sat}}S=\Delta n$, where Δn_{sat} is the saturation birefringence. The value for $\Delta n_{\mathrm{sat}}/\rho=3.8\times10^{-5}$ (mL/mg), where ρ is the concentration of virus in (mg/mL), as determined for *fd* via x-ray diffraction [13].

III. RESULTS

A. Effect of length and flexibility on the isotropic-nematic transition

Figure 3 presents the length dependence of the *I*-*N* coexistence concentrations at high (110 mM) and low (5 mM) ionic strength. For rigid rods $b_{\mathrm{eff}}c_i$, the dimensionless concentration of the isotropic phase in coexistence with the nematic phase, is predicted to be a constant, $b_{\mathrm{eff}}c_i=3.29$ [31], where $b_{\mathrm{eff}}=(\pi/4)L^2D_{\mathrm{eff}}$ and $c_i=\rho_iN_A/M$. In c_i, ρ_i is the isotropic mass density, N_A is Avogadro's number, and M is the molecular weight. Because the molecular weight is proportional to viral length, $M=M_{\mathrm{wt}}L/L_{\mathrm{wt}}$, with M_{wt} and L_{wt} equal to the molecular weight and length of wild type M13. Thus $b_{\mathrm{eff}}c_i=\rho_iLD_{\mathrm{eff}}[(\pi/4)L_{\mathrm{wt}}N_A/M]=25\rho_i$ (mg/mL)L (μm)D_{eff} (μm). Therefore, for rigid rods, $\rho_i=\mathrm{const}/L/D_{\mathrm{eff}}$, and at constant ionic strength (constant D_{eff}) ρ_i should be proportional to $1/L$. However, we observe that at a given ionic strength, the slope of ρ_i versus $1/L$ is not linear in Fig. 3, but instead increases with rod length, corresponding to an increase in $b_{\mathrm{eff}}c_i$. This is shown more clearly in Fig. 4, where $b_{\mathrm{eff}}c_i$ is plotted as a function of length. The increase in $b_{\mathrm{eff}}c_i$ with length is in agreement with predictions for rods of increasing flexibility (L/P), as shown by the theoretical curves from Khokhlov-Semenov theory and from SPT for semiflexible rods with a persistence length of $P=2.2$ μm. At high ionic strength ($I>60$ mM) we see good agreement with Khokhlov-Semenov theory calculated numerically by Chen (solid line) [6]. However, with decreasing ionic strength, we measure an increase in the flexibility dependence of $b_{\mathrm{eff}}c_i$. Subsequently, Khokhlov-Semenov theory only qualitatively describes the experimental results at low ionic strength. Agreement of the hard-rod Khokhlov-Semenov theory with our data is better at high ionic strength than at low ionic strength because the range of electrostatic interactions is weaker and L/D_{eff} is large, making the second virial approximation valid.

To interpret the observed increase in flexibility dependence of the phase transition with decreasing ionic strength, we turn to the scaled particle theory. The method for determining the scaled particle theoretical coexistence concentrations and nematic order parameters is described elsewhere [14]. In Fig. 4, we present the predicted SPT isotropic coexistence concentrations for rods with a diameter of 10.4 nm (110 mM ionic strength) and 29.4 nm (10 mM ionic strength). At high ionic strength, SPT shows fair agreement with experimental results, and the theoretical curve for $b_{\mathrm{eff}}c_i$ is close to that predicted by Chen for the infinitely long rod limit. Additionally, we observe in Fig. 4 that SPT indeed predicts a small dependence of $b_{\mathrm{eff}}c_i$ on L/D_{eff}, in contrast to the L/D_{eff} independent second virial theory. This suggests that the effective aspect ratio of the rods, which decreases with ionic strength, has a small effect on the *I*-*N* transition

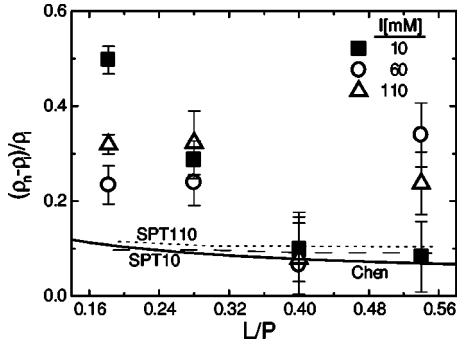

FIG. 5. Width, $(\rho_n-\rho_i)/\rho_i$, of the coexistence region as a function of rod flexibility L/P. Results are plotted for three ionic strengths (10 mM, 60 mM, and 110 mM). Solid line is due to Chen for rods with $P=2.2$ μm [6]. Dotted and dashed lines are due to scaled particle theory for M13 rods ($q=7e/\mathrm{nm}$) with a hard diameter D_{eff} at 110 mM (SPT110) and 10 mM (SPT10) ionic strength, respectively. For rigid rods, the Onsager prediction for the *I-N* coexistence width is 0.29 [1,8]. The width of the coexistence region should decrease with increasing flexibility.

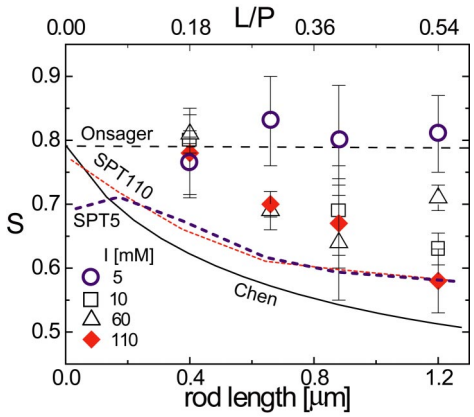

FIG. 6. (Color online) Nematic order parameter at coexistence as a function of rod length for four different ionic strengths. Solid black line represents the theoretical calculation by Chen [6] for the order parameter as a function of flexibility (L/P) indicated by the scale on the top of the graph. The dashed line is the theoretical nematic order parameter for rigid rods, $S=0.79$ [1,8]. The scaled particle curves (dotted lines) are calculated as in [13] for virus rods at 110 mM (SPT110) and 5 mM (SPT5) ionic strength. Theoretical curves were calculated for rods with a persistence length of 2.2 μm. The measured order parameter decreases with increasing particle length at high ionic strength, but remains constant at low ionic strength.

concentration. However, the L/D_{eff} dependence predicted by SPT is opposite the trend experimentally observed; increasing D_{eff}, by lowering ionic strength, increases the measured $b_{\mathrm{eff}}c_i$ but lowers the scaled particle theory $b_{\mathrm{eff}}c_i$. We argue that this discrepancy between scaled particle theory and experimental results at low ionic strength is due to the approximate treatment of electrostatics in D_{eff}, which is used not only as the theoretical hard rod diameter in SPT but also scales the experimental coexistence concentrations from ρ_i to $b_{\mathrm{eff}}c_i$. D_{eff} is determined from using the second virial coefficient, and therefore is not necessarily accurate beyond that limit, i.e., at low ionic strength. We note that the rescaled experimental coexistence concentrations, $b_{\mathrm{eff}}c_i$, are extremely sensitive to the value of D_{eff} used to rescale the measured coexistence concentrations, ρ_i. Differences in D_{eff} are translated linearly to changes in the experimental $b_{\mathrm{eff}}c_i$ by $b_{\mathrm{eff}}c_i=25\rho_i$ (mg/mL)L (μm)D_{eff} (μm). However, the predicted effect of changing L/D_{eff} on $b_{\mathrm{eff}}c_i$, as shown by the SPT curves in Fig. 4, is much smaller than the measured change in $b_{\mathrm{eff}}c_i$ with ionic strength. Agreement between SPT and our experimental results improves if the effective diameter at low ionic strength is smaller than predicted at the second virial limit.

The width of the coexistence region, $(\rho_n-\rho_i)/\rho_i$, was also measured and is presented in Fig. 5. At low ionic strength, the coexistence width qualitatively follows the decrease expected for increasing flexibility shown by the solid line due to Chen [6]. For most rod lengths, the value for the coexistence width is larger than predicted by both Khokhlov-Semenov theory and by scaled particle theory. At short rod lengths, this discrepancy is most likely due to the intrinsic bidispersity of the suspensions, which acts to widen the coexistence region [25]. A slow increase in the coexistence concentrations with time (possibly due to bacterial growth) [30] contributes to the large error bars, making comparison to predictions difficult. Above 10 mM ionic strength, where we see strong agreement between measurements of the coexistence concentrations and theoretical predictions, it is not apparent that there is any flexibility or ionic strength dependence in the width measurements.

The nematic order parameter obtained from measurements of the birefringence of the magnetically unwound and aligned cholesteric phase in coexistence with the isotropic phase is presented in Fig. 6. We observe that at high ionic strengths, the nematic order parameter decreases with increasing length (increasing flexibility) in qualitative agreement with Khokhlov-Semenov theory calculated by Chen [6]. With decreasing ionic strength, however, the measured nematic order parameter increases, approaching Onsager's rigid-rod predictions, due to increasing the range of electrostatic interactions. This has also been observed for *fd* virus suspensions [13]. Furthermore, at very low ionic strength (5 mM ionic strength) the nematic order parameter becomes independent of rod length and equal to the predicted rigid rod value of $S=0.8$. Scaled particle theory, as illustrated in Fig. 6, predicts that the nematic order parameter is largely independent of ionic strength. This suggests that the effective aspect ratio of the rods, which decreases with ionic strength, does not effect the nematic ordering. In addition, SPT agrees with the experimental measurements at high ionic strength better than Khokhlov-Semenov theory.

Another possible explanation for an increase in nematic order parameter with decreasing ionic strength is electrostatic stiffening. If the interparticle interactions are dominated by electrostatics, the flexibility of the rods might be screened. This effective "electrostatic persistence length" P_{el}, which makes a charged polymer more rigid when in solution, is a dominant effect in determining the flexibility of charged flexible polymers with $L/P\gg 1$. However, for the semiflexible M13 and *fd*, P_{el} is predicted to be less than 1% larger

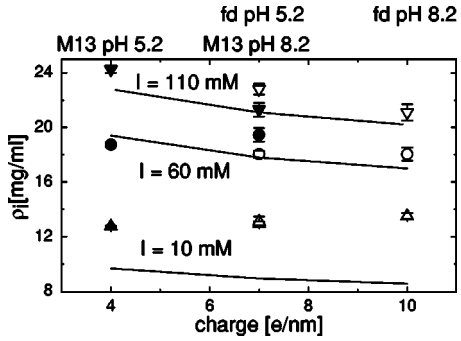

FIG. 7. Coexisting isotropic phase concentrations ρ_i as a function of particle surface charge for three ionic strengths, 10 mM, 60 mM, and 110 mM. Solid symbols are wild type M13 and open symbols are *fd* suspensions. Suspension *p*H is labeled above the graph for M13 and *fd* samples. Solid line is from scaled particle theory for semiflexible hard rods with a diameter D_{eff} and $L/P=0.4$. The charge dependence of the phase transition is well described by theory for ionic strengths of 60 mM and 110 mM.

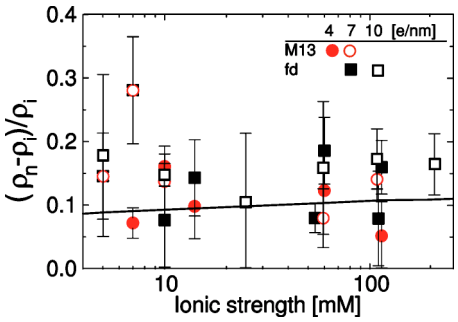

FIG. 8. (Color online) Width of the isotropic-nematic coexistence region for wild type M13 and *fd* rods at three different surface charges as a function of ionic strength. Both M13 and *fd* have a length of $L=0.88$ μm. Solid symbols are at *p*H 5.2 and open symbols are at *p*H 8.2 for M13 (circles) and *fd* (squares) suspensions. Solid line is from scaled particle theory for hard semiflexible rods with $L/P=0.4$ and is independent of rod surface charge. The Onsager prediction for the *I-N* coexistence width in dimensionless units of *bc* for hard rigid rods is $(4.19-3.29)/3.29=0.29$ [1,8]. The coexistence width does not clearly show any charge dependence.

than the bare persistence length [32]. Additionally, the results for the coexistence concentrations presented in Fig. 4 indicate that with decreasing ionic strength, the measured coexistence concentrations deviate further from Onsager's rigid-rod predictions. Thus the measured coexistence concentrations and nematic order parameters exhibit contradictory trends, away from Onsager's rigid rod prediction versus towards Onsager's rigid rod prediction, respectively, with decreasing ionic strength. Therefore, electrostatic stiffening of the polymer cannot account for the observed high values of the order parameter at low ionic strength. Neither scaled particle theory nor variation in the electrostatic persistence length satisfactorily explain the low ionic strength data.

B. Effect of viral surface charge on the isotropic-nematic transition

In this section, we compare the phase behavior of M13 virus to that of *fd* virus as a function of surface charge and ionic strength. Recall that these particles have the same length $L=0.88$ μm and persistence length $P=2.2$ μm. In Fig. 7, we present measurements of the isotropic coexistence concentrations as a function of viral surface charge at high and low ionic strength. The theoretical curve is from scaled particle theory for charged, semiflexible rods with $L/P=0.4$. We only present the theoretical results from scaled particle theory in this section as this theory should more accurately describe the finite-length rod phase behavior than the second virial theory. In Fig. 7, we confirm that the charge dependence of the *I-N* coexistence concentrations is accurately described by scaled particle theory at high ionic strengths. However, the efficacy of D_{eff} as a means for incorporating all electrostatic interactions again diminishes at low ionic strength ($I<60$ mM), as seen previously in Fig. 4 and in Fig. 6.

Figure 8 presents the width of the coexistence region as a function of charge and ionic strength. The width of the coexistence region is independent of the surface charge of the rods and agrees (within large error bars) with scaled particle

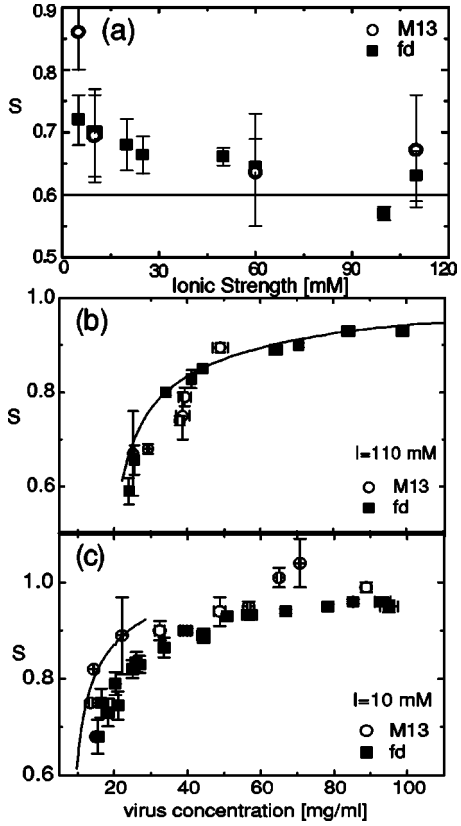

FIG. 9. Order parameter of the nematic phase (a) coexisting with the isotropic phase as a function of ionic strength (b) as a function of concentration at 110 mM ionic strength and (c) as a function of concentration at 10 mM ionic strength *p*H 8.2. Values for M13 were obtained by birefringence measurements and values for *fd* were obtained previously by x-ray diffraction [13]. Solid lines are scaled particle theory for semiflexible hard rods of diameter D_{eff} and $L/P=0.4$. The order parameters for M13 agree with those measured for *fd* independent of concentration and ionic strength.

theory predictions. Both the measured coexistence concentrations and coexistence widths show that the effect of surface charge on the electrostatic interactions which drive the *I-N* phase transition are weak, which is consistent with the idea of charge renormalization incorporated into the calculations of D_{eff}.

Nematic order parameters obtained from measurements of the birefringence of magnetically unwound and aligned cholesteric samples of M13 at *p*H 8.2 are compared to previous measurements of *fd* suspension nematic order parameters, measured via x-ray diffraction techniques, also at *p*H 8.2 [13], in Fig. 9. Recall that the nematic order parameter of *fd* is known to be proportional to the birefringence of the suspension by the relationship $S=\Delta n/\Delta n_{\mathrm{sat}}$, where $\Delta n_{\mathrm{sat}}=3.8\times10^{-5}$ mL/mg [13]. The order parameter of M13 was measured at *I-N* coexistence as a function of ionic strength, and deep within the nematic phase for high (110 mM) and low (10 mM) ionic strength. Theoretical predictions from scaled particle theory for the nematic order parameter of hard semiflexible rods with $L/P=0.4$ are also shown in Fig. 9. The order parameters of M13 and *fd* were found to be equal as a function of ionic strength and concentration, indicating that the surface charge difference of 30% between the two particles does not affect nematic ordering. The insensitivity of the nematic order parameter to surface charge is consistent with the surface charge renormalization incorporated into D_{eff} calculations (Fig. 1) [3]. The strong agreement of M13 and *fd* order parameters also indicates that these two different virus particles have the same birefringence per particle, $\Delta n_{\mathrm{sat}}=3.8\times10^{-5}$ mL/mg [13]. Additionally, we again observe that the scaled particle theory fits the measured order parameter best for high ionic strength data.

IV. CONCLUSION

At high ionic strengths, where the range of electrostatic interactions is small and L/D_{eff} is large, the isotropic-nematic transition of the experimental system of charged semiflexible bacteriophages is well described by Khokhlov-Semenov theory for semiflexible charged rods. Increasing flexibility increases the coexistence concentrations $b_{\mathrm{eff}}c_i$ (Fig. 4) and lowers the nematic order parameter (Fig. 6). In the region of high ionic strength, D_{eff} accurately describes both the charge dependence and ionic strength dependence of the isotropic-nematic phase transition (Fig. 7). At low ionic strength, however, we find that the *I-N* coexistence concentrations and the nematic order parameter do not agree with theoretical predictions from either Onsager's second virial theory or scaled particle theory. At low ionic strength, the flexibility dependence of the nematic order parameter is much weaker than expected (Fig. 6), but the flexibility dependence of the coexistence concentrations is much stronger than expected (Fig. 4). Because of these contradictory results, we suggest that the disagreement between theoretical predictions and experimental data at low ionic strength is due to the approximate incorporation of the electrostatic interactions into the theoretical free energy via D_{eff}.

ACKNOWLEDGMENTS

We would like to thank Zvonimir Dogic for the program which calculates the scaled particle theory phase diagram. We also acknowledge support from the National Science Foundation (Grant No. DMR-CMP 0088008).

[1] L. Onsager, Ann. N.Y. Acad. Sci. **51**, 627 (1949).
[2] A. R. Khokhlov and A. N. Semenov, Physica A **112**, 605 (1982).
[3] J. Tang and S. Fraden, Liq. Cryst. **19**, 459 (1995).
[4] T. Sato and A. Teramoto, Adv. Polym. Sci. **126**, 85 (1996).
[5] A. Grosberg and A. Khokhlov, *Giant Molecules: Here, There and Everywhere* (Academic, New York, 1997).
[6] Z. Y. Chen, Macromolecules **26**, 3419 (1993).
[7] R. F. Kayser, Jr. and H. J. Raveche, Phys. Rev. A **17**, 2067 (1978).
[8] J. Herzfeld, A. E. Berger, and J. W. Wingate, Macromolecules **17**, 1718 (1984).
[9] A. Stroobants, H. N. W. Lekkerkerker, and T. Odijk, Macromolecules **19**, 2232 (1986).
[10] J. R. Philip and R. A. Wooding, J. Chem. Phys. **52**, 953 (1970).
[11] J. P. Straley, Mol. Cryst. Liq. Cryst. **24**, 7 (1973).
[12] M. A. Cotter, in *The Molecular Physics of Liquid Crystals*, edited by G. R. Luckhurst and G. W. Gray (Academic, London, 1979), pp. 169–189.
[13] K. R. Purdy, Z. Dogic, S. Fraden, A. Rühm, L. Lurio, and S. G. J. Mochrie, Phys. Rev. E **67**, 031708 (2003).
[14] Z. Dogic, K. Purdy, E. Grelet, M. Adams, and S. Fraden, Phys. Rev. E **69**, 051702 (2004).
[15] J. Lapointe and D. A. Marvin, Mol. Cryst. Liq. Cryst. **19**, 269 (1973).
[16] Z. Dogic and S. Fraden, Phys. Rev. Lett. **78**, 2417 (1997).
[17] Z. Dogic and S. Fraden, Philos. Trans. R. Soc. London, Ser. A **359**, 997 (2001).
[18] P. G. de Gennes and J. Prost, *The Physics of Liquid Crystals*, 2nd ed. (Oxford University Press, Oxford, 1974).
[19] K. R. Purdy and S. Fraden (unpublished).
[20] S. Fraden, in *Observation, Prediction, and Simulation of Phase Transitions in Complex Fluids*, edited by M. Baus, L. F. Rull, and J. P. Ryckaert (Kluwer, Dordrecht, 1995), pp. 113–164.
[21] D. A. Marvin, R. D. Hale, C. Nave, and M. H. Citterich, J. Mol. Biol. **235**, 260 (1994).
[22] K. Zimmermann, J. Hagedorn, C. C. Heuck, M. Hinrichsen, and J. Ludwig, J. Biol. Chem. **261**, 1653 (1986).
[23] M. J. Glucksman, S. Bhattacharjee, and L. Makowski, J. Mol. Biol. **226**, 455 (1992).
[24] J. Sambrook, E. F. Fritsch, and T. Maniatis, in *Molecular Cloning: A Laboratory Manual*, 2nd ed. (Cold Spring Harbor Laboratory Press, Cold Spring Harbor, NY, 1989), Chap. 4.
[25] H. N. W. Lekkerkerker, P. Coulon, V. der Haegen, and R. Deblieck, J. Chem. Phys. **80**, 3427 (1984).
[26] T. Sato and A. Teramoto, Acta Polym. **45**, 399 (1994).
[27] J. T. G. Overbeek, in *Advances in Colloid Science*, edited by

H. Mark and E. J. W. Verwey (Interscience Publishers, New York, 1950), pp. 97–135.
[28] R. Oldenbourg and W. C. Phillips, Rev. Sci. Instrum. **57**, 2362 (1986).
[29] J. Torbet and G. Maret, Biopolymers **20**, 2657 (1981).
[30] J. Tang and S. Fraden, Phys. Rev. Lett. **71**, 3509 (1993).
[31] E. M. Kramer and J. Herzfeld, Phys. Rev. E **58**, 5934 (1998).
[32] T. Odijk and A. C. Houwaart, J. Polym. Sci., Polym. Phys. Ed. **16**, 627 (1978).